Supplementary materials

Ferrocene-containing tin(IV) complexes based on o-benzoquinone and o-iminobenzoquinone ligands. Synthesis, molecular structure and electrochemical properties

Svetlana V. Baryshnikova[†], Andrey I. Poddel'sky[†,*], Ekaterina V. Bellan[†], Ivan V. Smolyaninov[‡,§], Anton V. Cherkasov[†], Georgy K. Fukin[†], Nadezhda T. Berberova[§], Vladimir K. Cherkasov[†], Gleb A. Abakumov[†]

[†] *G.A. Razuvaev Institute of Organometallic Chemistry, Russian Academy of Sciences, 603137, Tropinina str. 49, Nizhny Novgorod, Russia*

[‡] *Federal Sate Budgetary Institution of Science "Federal Research Centre the Southern Scientific Centre of the Russian Academy of Sciences", 344006, Chehova av. 41, Rostov-on-Don, Russia*

[§] *Astrakhan State Technical University, 414025, Tatisheva str. 16, Astrakhan, Russia*

Content:

Table S1. Crystallographic data and structures refinement details for **5**, **7** and **9**·toluene.

Compound	**5** (Fc-4,6-IP)$_2$Sn(4,5-Cl$_2$-3,6-Cat)	**7** (Fc-4,6-IP)$_2$Sn(AP-Me)	**9**·toluene (Fc-4,6-IP)$_2$Sn(AP-iPr), Toluene
Formula	$C_{64}H_{78}Cl_2Fe_2N_2O_4Sn$	$C_{72}H_{89}Fe_2N_3O_3Sn$	$C_{76}H_{97}Fe_2N_3O_3Sn$, C_7H_8
M	1240.57	1274.85	1423.08
Crystal system	Triclinic	Monoclinic	Monoclinic
Space group	*P–1*	*P2$_1$/n*	*P2$_1$/c*
a (Å)	12.0499(6)	13.929(4)	11.3663(14)
b (Å)	13.9061(7)	22.042(6)	46.539(6)
c (Å)	18.4879(10)	21.031(8)	14.2559(19)
α (°)	90.3520(10)	90	90
β (°)	94.3550(10)	96.582(7)	108.578(2)
γ (°)	108.2720(10)	90	90
V (Å^3)	2931.8(3)	6415(4)	7148.2(16)
Z	2	4	4
d_{calc} (g cm^{-3})	1.405	1.320	1.322
μ (mm^{-1})	1.051	0.881	0.798
F_{000}	1288	2672	3000
Crystal size (mm)	0.18 × 0.13 × 0.12	0.22 × 0.11 × 0.01	0.46 × 0.26 × 0.06
θ range for data collection (°)	2.20–30.10	1.67–25.08	2.30–24.80
Reflections collected / unique (R_{int})	42854 / 17188 (0.0303)	50627 / 11369 (0.1320)	54861 / 12201 (0.0499)
Data / restraints / parameters	17188 / 96 / 722	11369 / 0 / 750	12201 / 0 / 788
$S(F^2)$	1.040	1.006	1.069
R ($I > 2\sigma(I)$)	R_1 = 0.0366,wR_2 = 0.0847	R_1 = 0.0524, wR_2 = 0.1011	R_1 = 0.0608, wR_2 = 0.1264
R (all data)	R_1 = 0.0482, wR_2 = 0.0896	R_1 = 0.1073, wR_2 = 0.1237	R_1 = 0.0704, wR_2 = 0.1304
Largest diff. peak and hole (e Å^{-3})	1.12 / –0.73	0.91 / –0.78	0.92 / –1.10

Table S2. The selected bond lengths (Å) and angles (°) in **5**, **7** and **9**.

5		**7**		**9**	
Bond	bond lengths, Å	Bond	bond lengths, Å	Bond	bond lengths, Å
Sn(1)-O(1)	2.021(2)	Sn(1)-O(1)	2.053(3)	Sn(1)-O(1)	2.049(3)
Sn(1)-O(2)	2.027(2)	Sn(1)-O(2)	2.022(3)	Sn(1)-O(2)	2.032(3)
Sn(1)-O(3)	2.023(2)	Sn(1)-O(3)	2.036(3)	Sn(1)-O(3)	2.024(3)
Sn(1)-O(4)	2.031(2)	Sn(1)-N(1)	2.220(4)	Sn(1)-N(1)	2.235(4)
Sn(1)-N(1)	2.177(2)	Sn(1)-N(2)	2.279(4)	Sn(1)-N(2)	2.271(4)
Sn(1)-N(2)	2.193(2)	Sn(1)-N(3)	2.052(4)	Sn(1)-N(3)	2.077(4)
O(3)-C(51)	1.351(2)	O(3)-C(51)	1.378(5)	O(3)-C(51)	1.359(5)
O(4)-C(52)	1.354(2)	N(3)-C52)	1.398(6)	N(3)-C(52)	1.407(6)
C(51)-C(56)	1.394(3)	C(51)-C(52)	1.415(7)	C(51)-C(52)	1.419(7)
C(51)-C(52)	1.428(3)	C(52)-C(53)	1.398(6)	C(52)-C(53)	1.385(6)
C(52)-C(53)	1.395(3)	C(53)-C(54)	1.398(7)	C(53)-C(54)	1.392(7)
C(53)-C(54)	1.415(3)	C(54)-C(55)	1.397(7)	C(54)-C(55)	1.380(7)
C(54)-C(55)	1.392(3)	C(55)-C(56)	1.405(7)	C(55)-C(56)	1.405(7)
C(55)-C(56)	1.415(3)	C(51)-C(56)	1.397(7)	C(51)-C(56)	1.392(7)
Cl(1)-C(54)	1.749(2)				
Cl(2)-C(55)	1.745(2)				
Angle, º		Angle, º		Angle, º	
O(1)-Sn(1)-O(2)	99.77(6)	O(1)-Sn(1)-O(2)	89.3(2)	O(1)-Sn(1)-O(2)	93.0(2)
O(1)-Sn(1)-O(3)	88.53(6)	O(1)-Sn(1)-O(3)	164.3(2)	O(1)-Sn(1)-O(3)	87.3(2)
O(2)-Sn(1)-O(3)	166.16(6)	O(2)-Sn(1)-O(3)	106.3(2)	O(2)-Sn(1)-O(3)	179.7(2)
O(1)-Sn(1)-O(4)	164.12(6)	O(1)-Sn(1)-N(1)	75.8(2)	O(1)-Sn(1)-N(1)	76.4(2)
O(2)-Sn(1)-O(4)	93.41(6)	O(2)-Sn(1)-N(1)	160.3(2)	O(2)-Sn(1)-N(1)	91.9(2)
O(3)-Sn(1)-O(4)	80.38(6)	O(3)-Sn(1)-N(1)	88.7(2)	O(3)-Sn(1)-N(1)	88.4(2)
O(1)-Sn(1)-N(1)	78.12(6)	O(1)-Sn(1)-N(2)	85.0(2)	O(1)-Sn(1)-N(2)	84.1(2)
O(2)-Sn(1)-N(1)	87.32(6)	O(2)-Sn(1)-N(2)	77.0(2)	O(2)-Sn(1)-N(2)	76.2(2)
O(3)-Sn(1)-N(1)	105.33(6)	O(3)-Sn(1)-N(2)	97.0(2)	O(3)-Sn(1)-N(2)	103.6(2)
O(4)-Sn(1)-N(1)	93.79(6)	O(1)-Sn(1)-N(3)	98.7(2)	O(1)-Sn(1)-N(3)	166.2(2)
O(1)-Sn(1)-N(2)	88.27(6)	O(2)-Sn(1)-N(3)	95.9(2)	O(2)-Sn(1)-N(3)	98.8(2)
O(2)-Sn(1)-N(2)	77.00(6)	O(3)-Sn(1)-N(3)	81.4(2)	O(3)-Sn(1)-N(3)	81.0(2)
O(3)-Sn(1)-N(2)	92.32(6)	N(1)-Sn(1)-N(2)	88.8(2)	N(1)-Sn(1)-N(2)	156.6(2)
O(4)-Sn(1)-N(2)	103.41(6)	N(1)-Sn(1)-N(3)	99.0(2)	N(3)-Sn(1)-N(1)	96.0(2)
N(1)-Sn(1)-N(2)	157.24(6)				

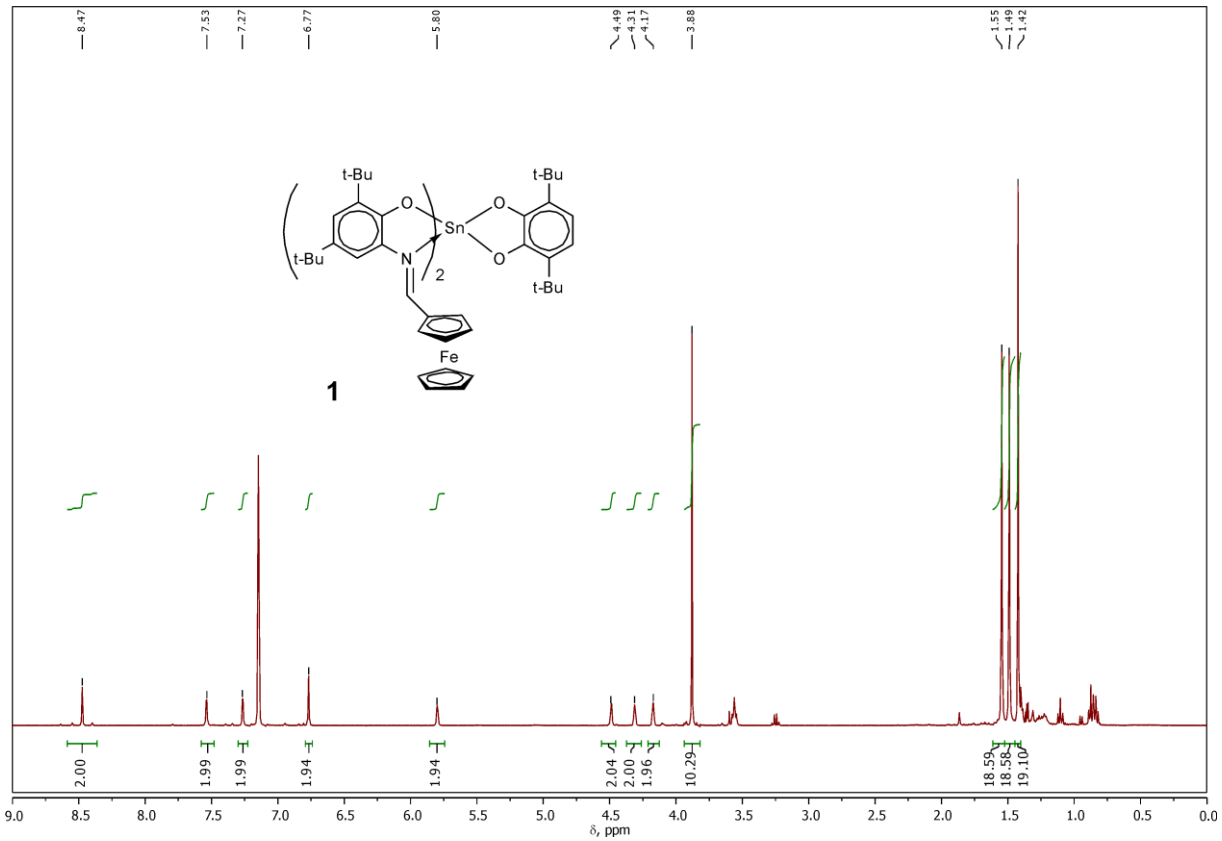

Figure S1. The ^{1}H NMR spectrum of (Fc-4,6-IP)$_2$Sn^{IV}(3,6-Cat) (**1**) (400 MHz, C_6D_6).

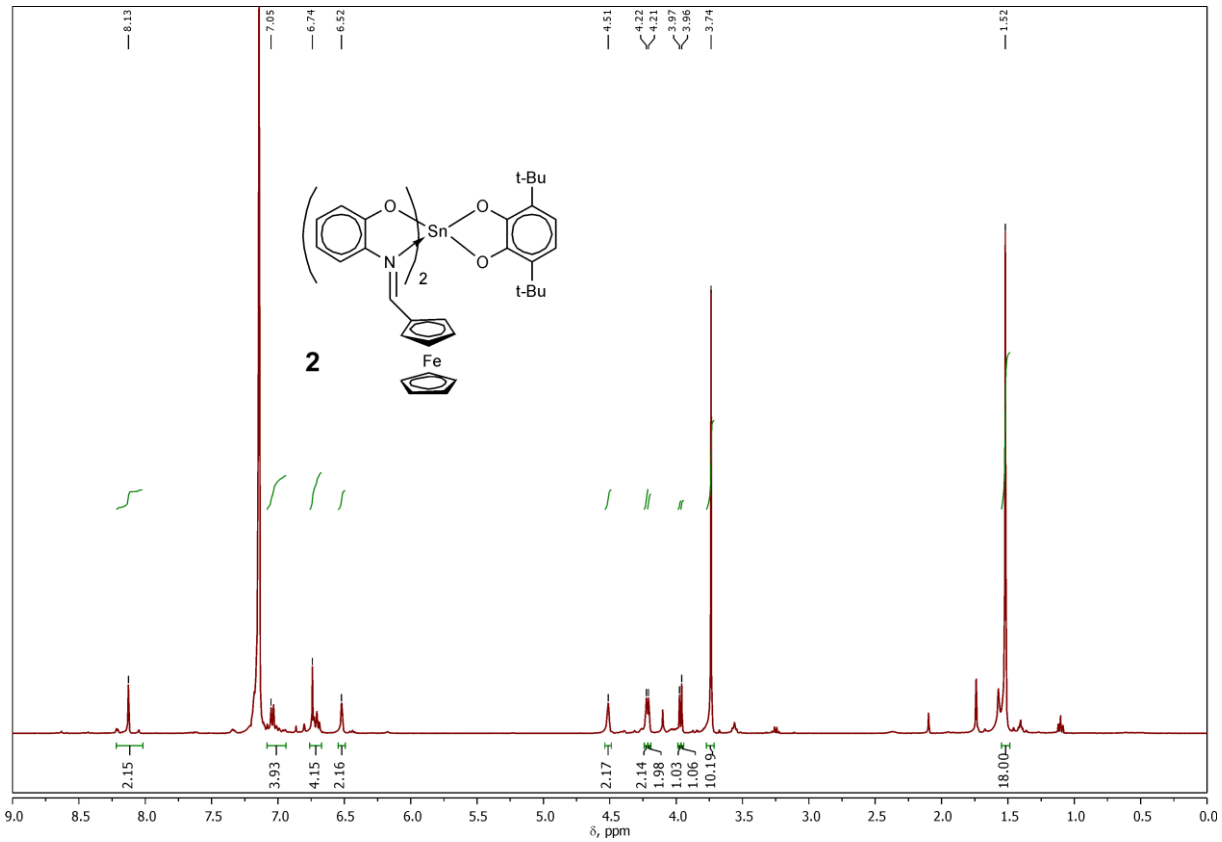

Figure S2. The ^{1}H NMR spectrum of (Fc-IP)$_2$Sn^{IV}(3,6-Cat) (**2**) (400 MHz, C_6D_6).

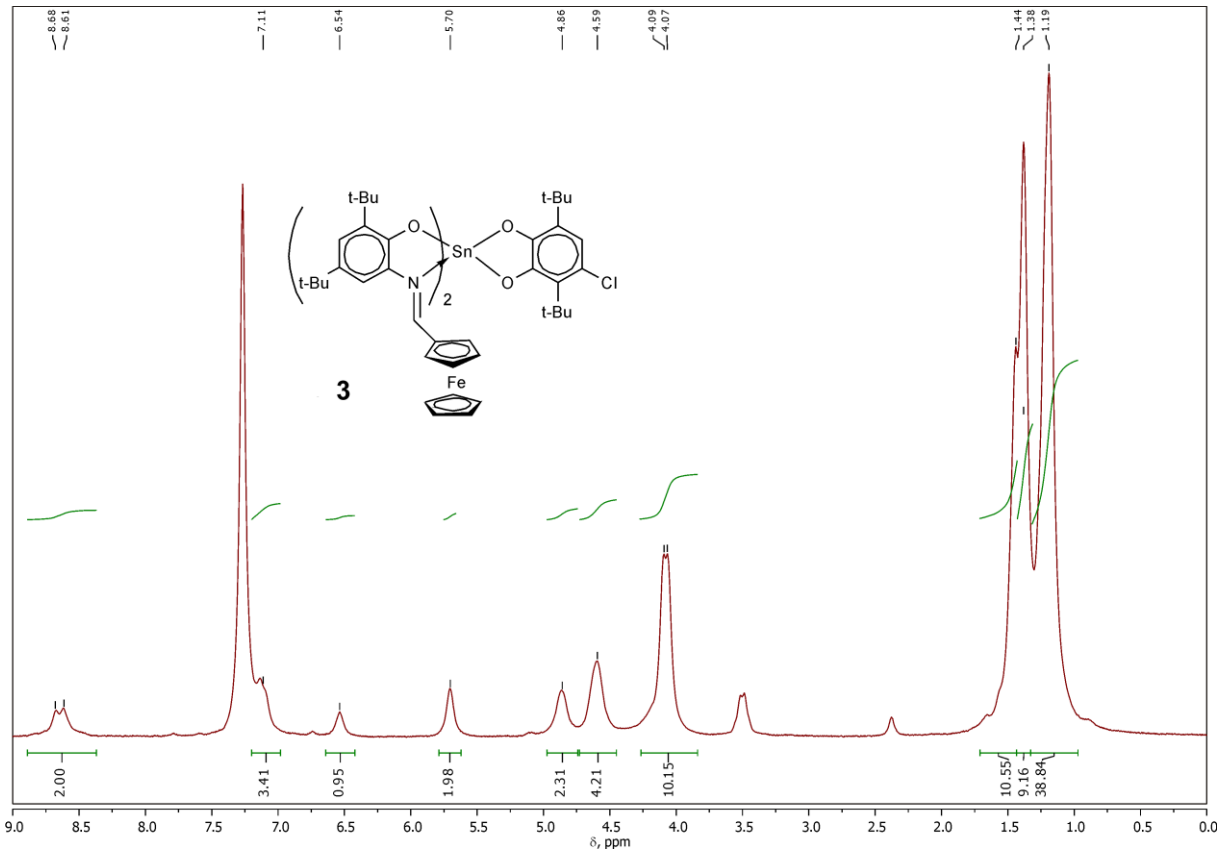

Figure S3. The ^{1}H NMR spectrum of (Fc-4,6-IP)$_2$Sn^{IV}(4-Cl-3,6-Cat) (**3**) (200 MHz, $CDCl_3$).

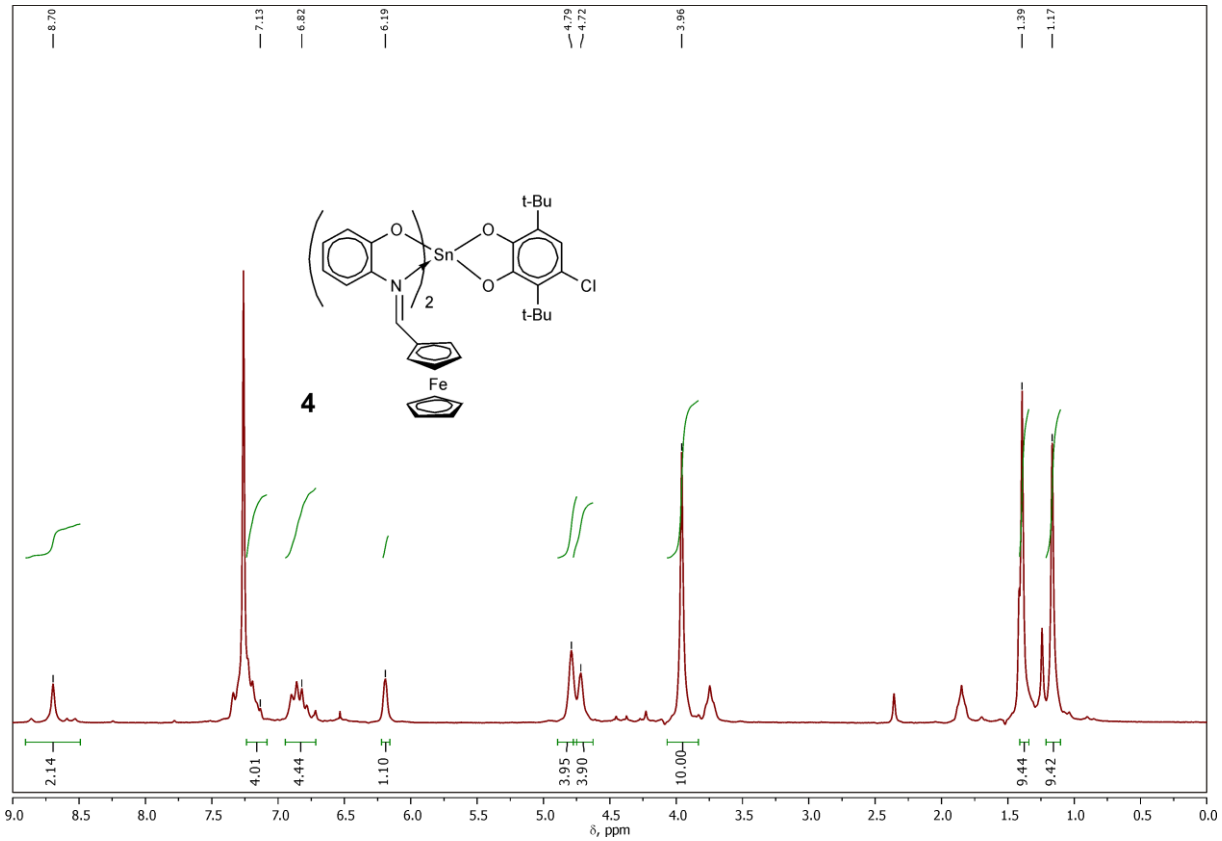

Figure S4. The ^{1}H NMR spectrum of (Fc-IP)$_2$Sn^{IV}(4-Cl-3,6-Cat) (**4**) (200 MHz, $CDCl_3$).

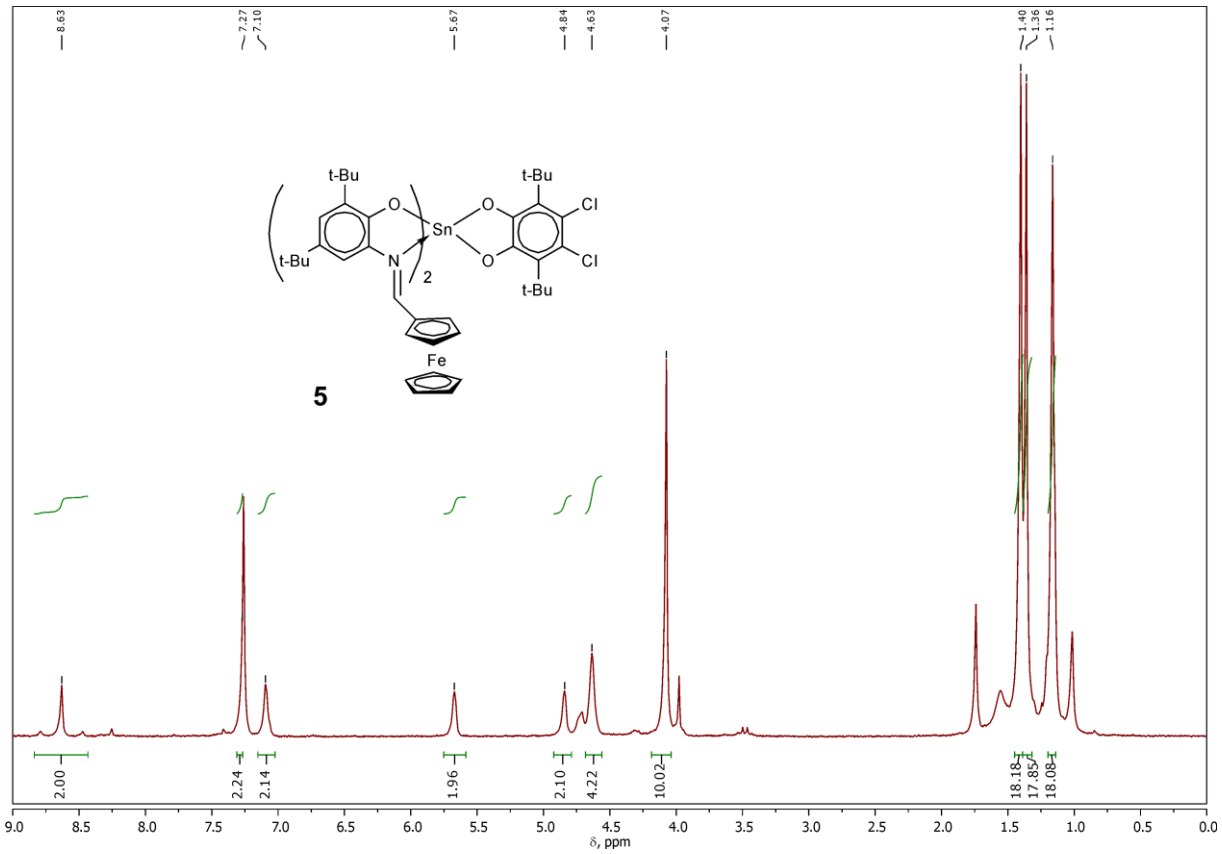

Figure S5. The ^{1}H NMR spectrum of (Fc-4,6-IP)$_2$Sn^{IV}(4,5-Cl$_2$-3,6-Cat) (**5**) (200 MHz, CDCl$_3$).

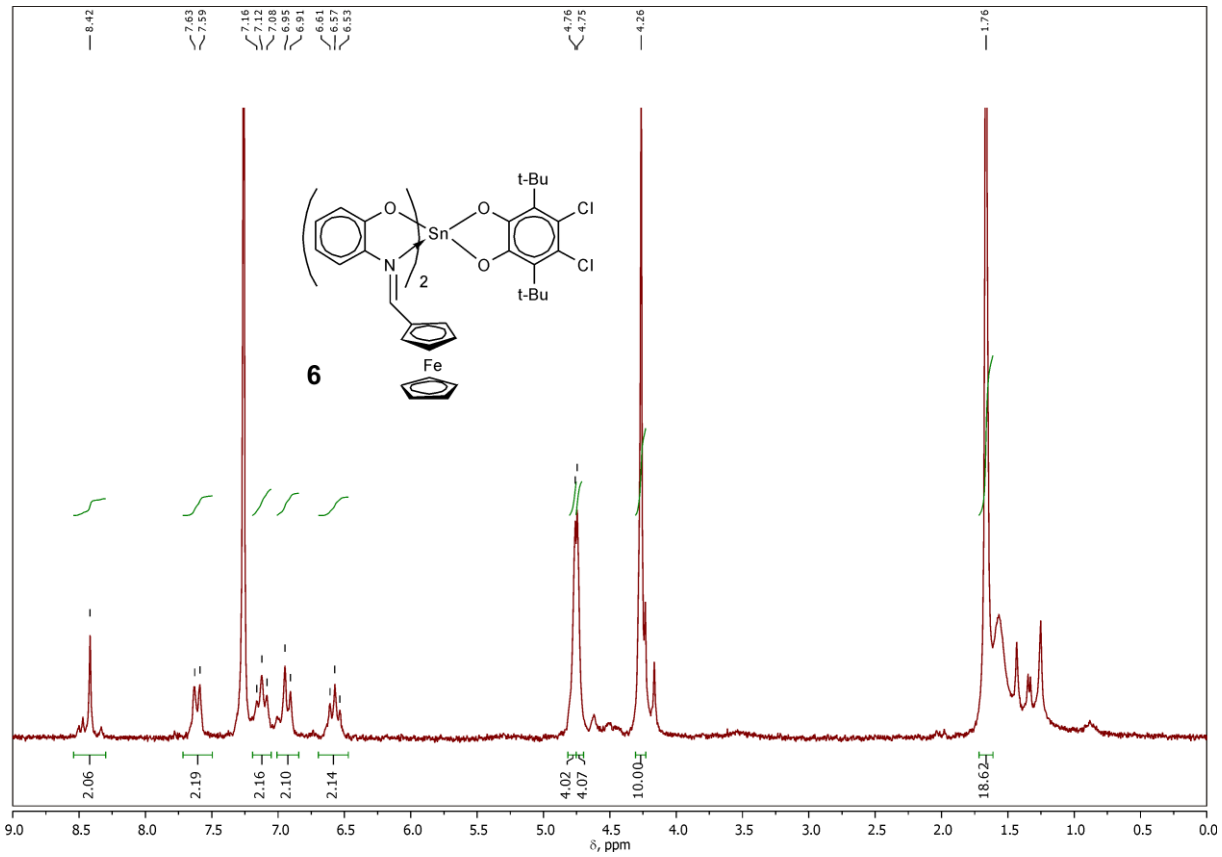

Figure S6. The ^{1}H NMR spectrum of (Fc-IP)$_2$Sn^{IV}(4,5-Cl$_2$-3,6-Cat) (**6**) (200 MHz, CDCl$_3$).

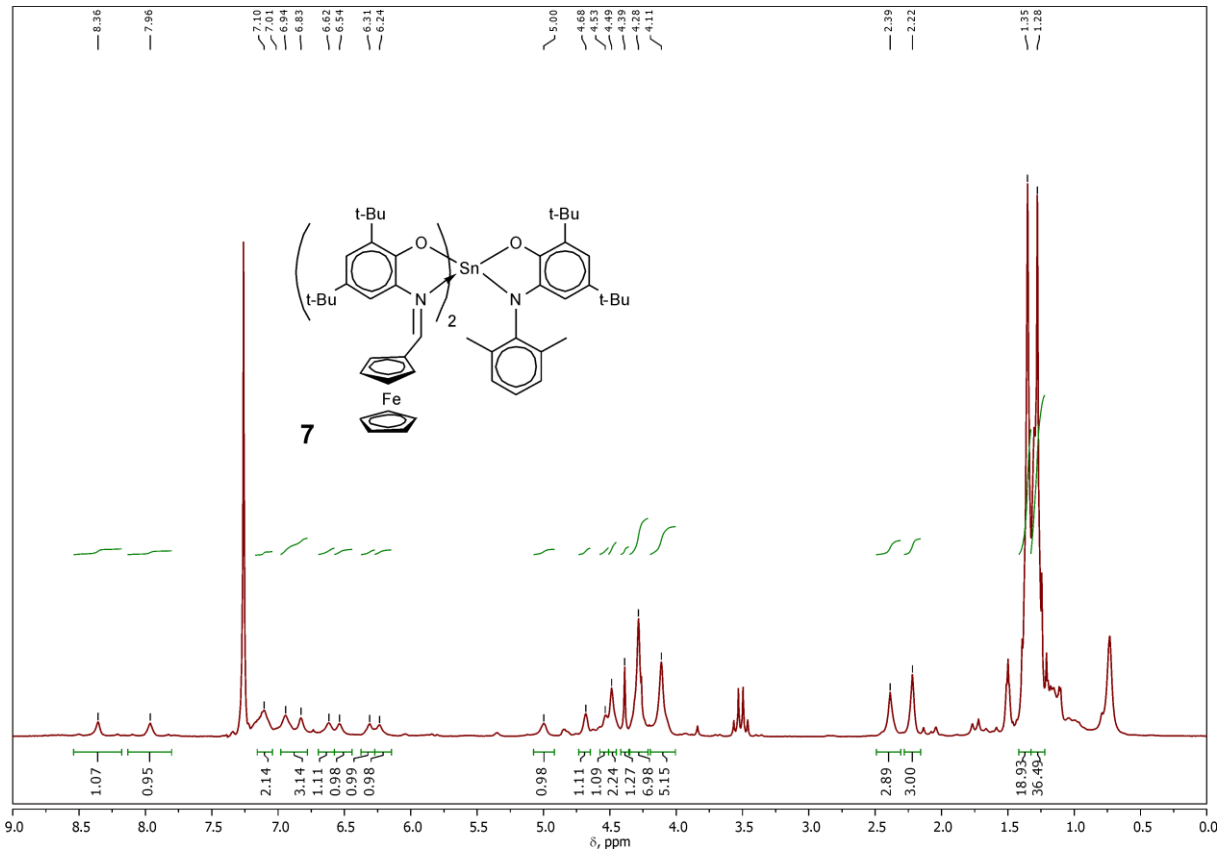

Figure S7. The ^{1}H NMR spectrum of (Fc-4,6-IP)$_2$Sn^{IV}(AP-Me) (**7**) (200 MHz, $CDCl_3$).

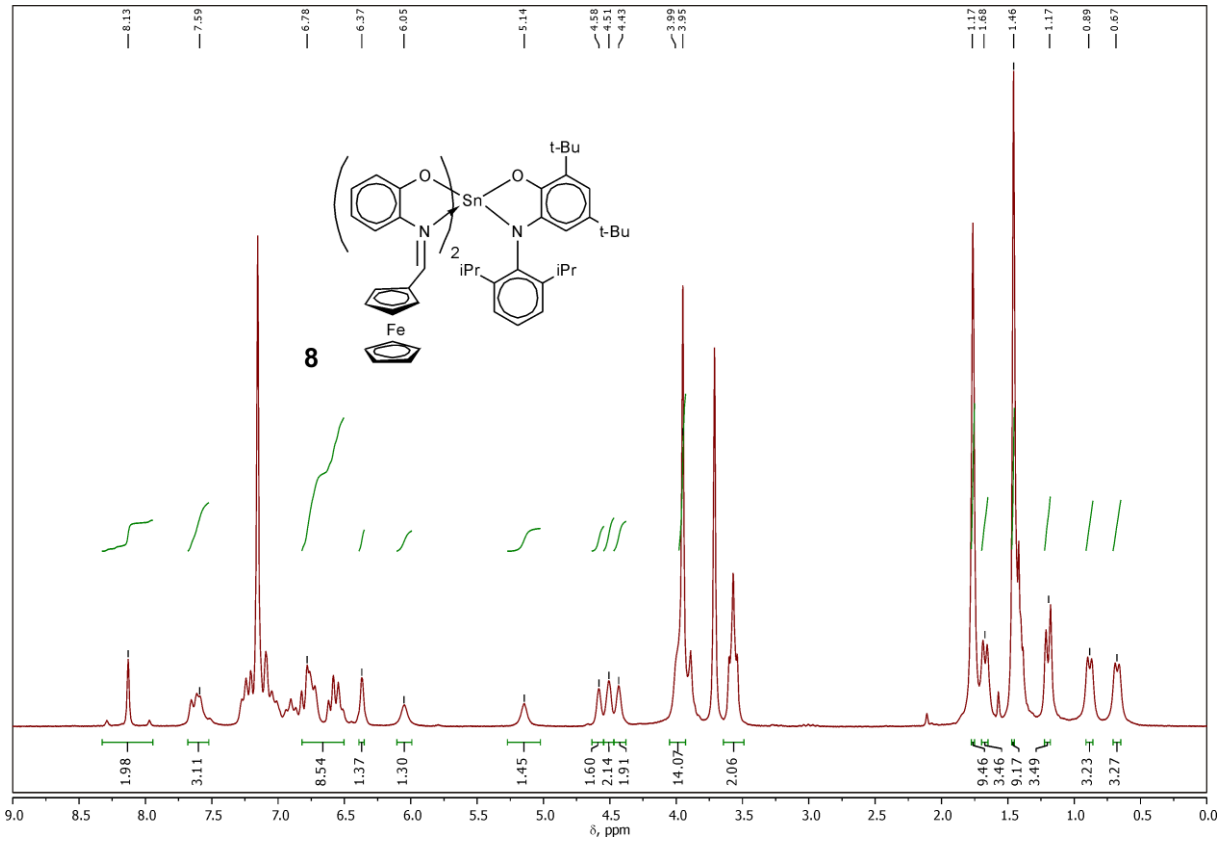

Figure S8. The ^{1}H NMR spectrum of (Fc-IP)$_2$Sn^{IV}(AP-iPr) (**8**) (200 MHz, C_6D_6).

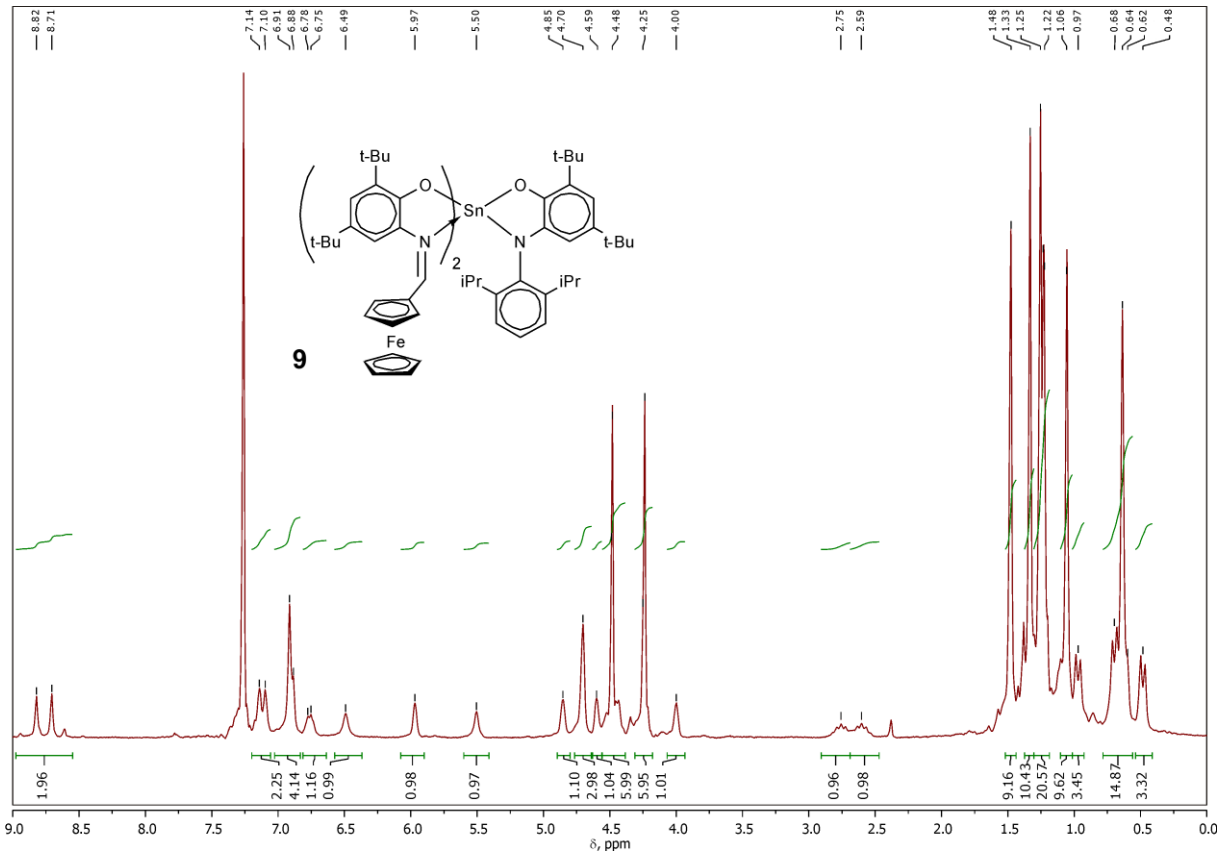

Figure S9. The ^{1}H NMR spectrum of (Fc-4,6-IP)$_2$Sn^{IV}(AP-iPr) (**9**) (200 MHz, $CDCl_3$).

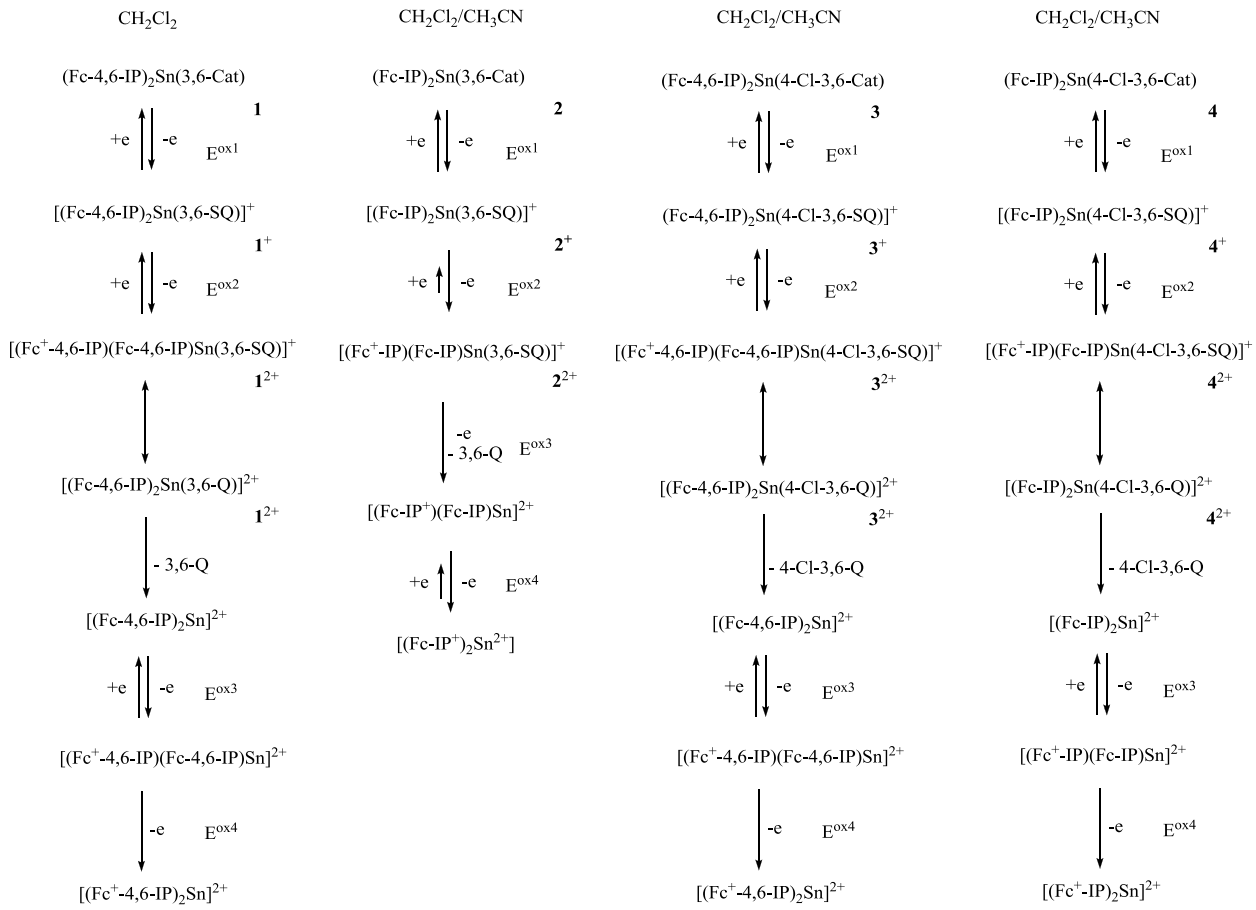

Scheme S1. The electrochemical oxidation of **1-4**.

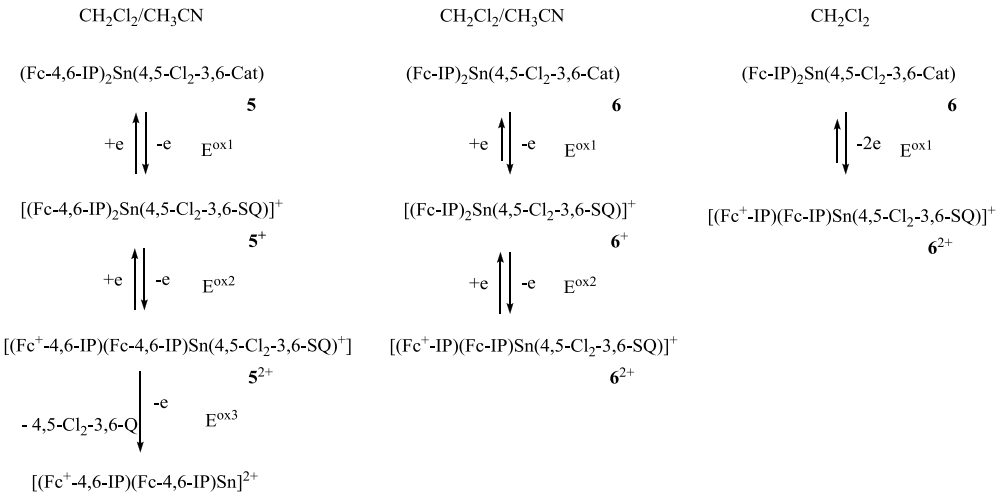

Scheme S2. The electrochemical oxidation of **5** and **6**.

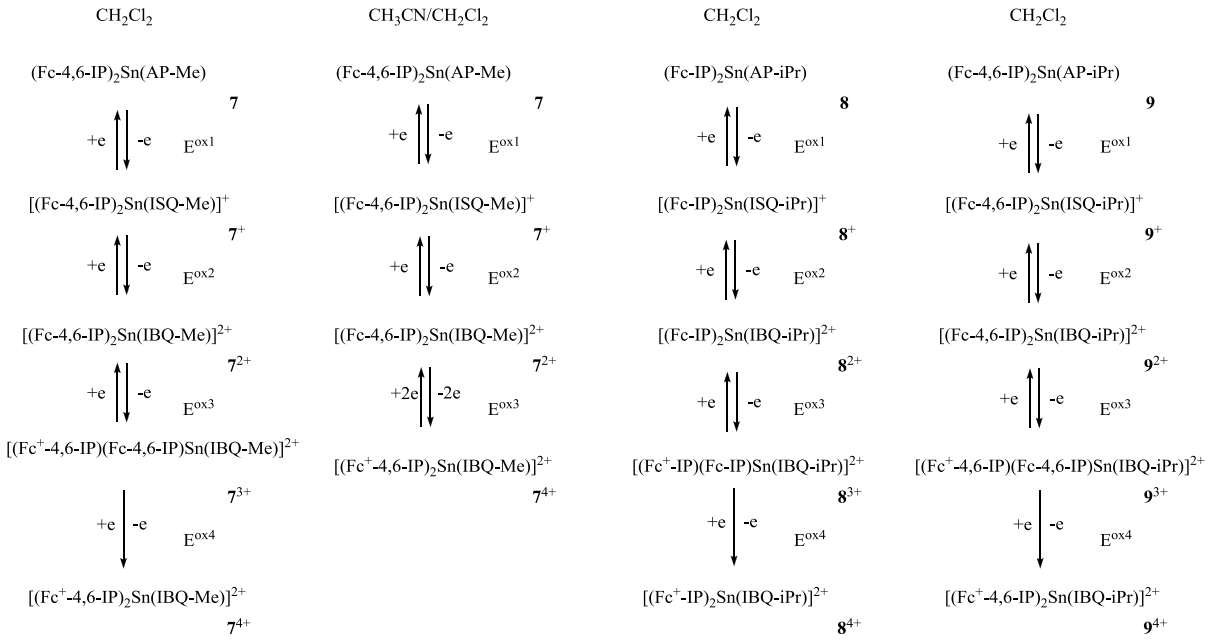

Scheme S3. The electrochemical oxidation of **7-9**.

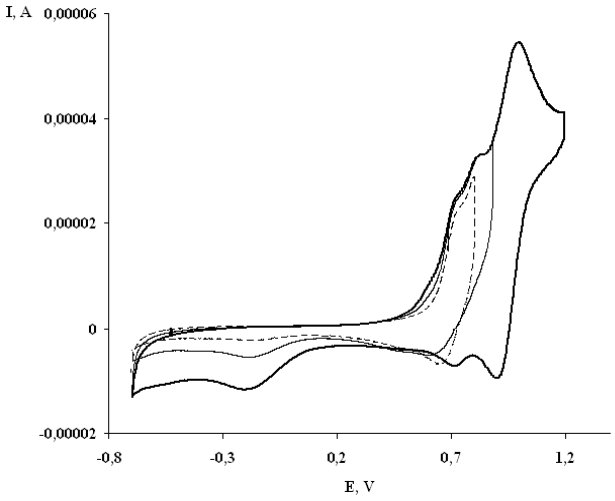

Figure S10. CVs of the oxidation of **2** at the potential sweep from –0.70 to +0.80 V (dotted line); at the potential sweep from –0.70 to +0.95 V (lean solid line); at the potential sweep from –0.70 to +1.20 V (bold solid line). Conditions: CH_3CN/CH_2Cl_2 (1:1), c = 1 mM, 0.1 M TBAP, scan rate 200 mV s^{-1}, T = 298 K.

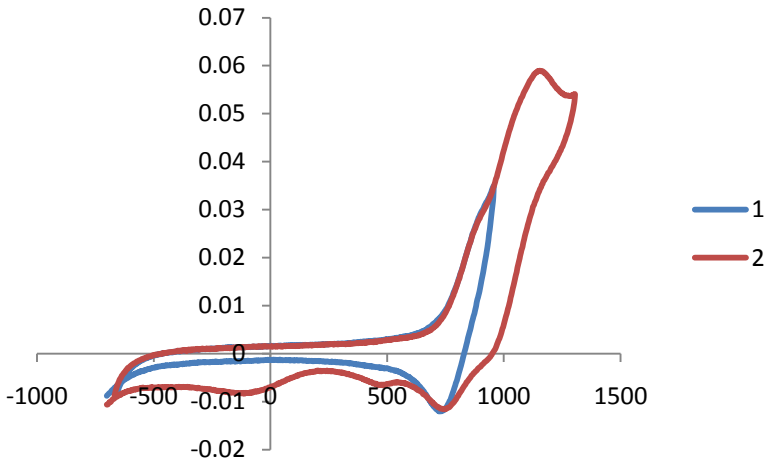

Figure S11. The CVs of the oxidation of **5**: (1) the potential sweep from –0.66 to +0.95 V; (2) the potential sweep from –0.67 to +1.05 V. Conditions: CH_2Cl_2, c = 1 mM, 0.1 M TBAP, scan rate 200 mV s^{-1}, T = 298 K.

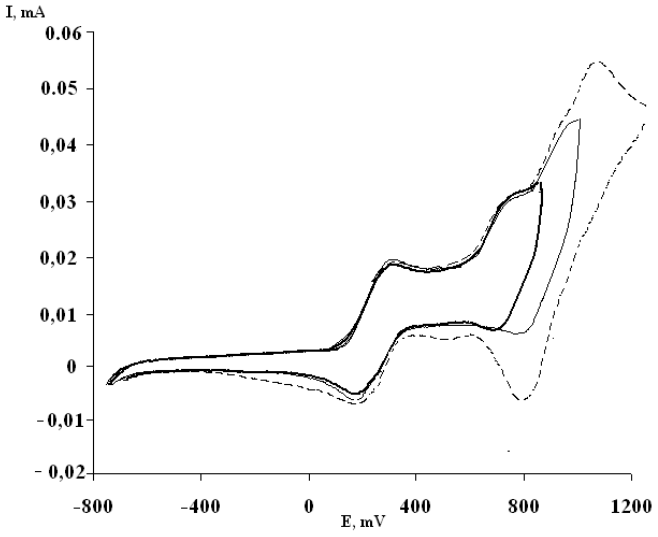

Figure S12. The CVs for the oxidation of **8**: (bold solid line) the potential sweep from -0.7 to +0.85 V; (lean solid line) the potential sweep from -0.7 to +1.05 V; (dotted line) the potential sweep from -0.7 to +1.20 V. Conditions: CH_2Cl_2, c = 1 mM, 0.1 M TBAP, scan rate 200 mV s^{-1}, T = 298 K.

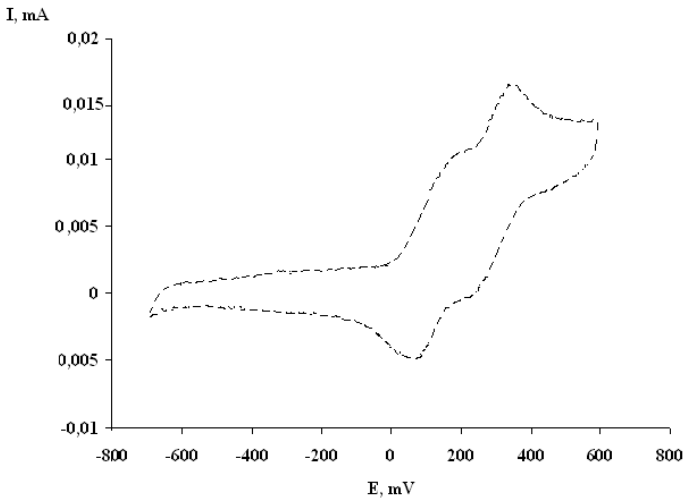

Figure S13. The CV of the oxidation of **9**: the potential sweep from -0.7 to +0.60 V. Conditions: CH_2Cl_2, c = 1 mM, 0.1 M TBAP, scan rate 200 mV s^{-1}, T = 298 K.

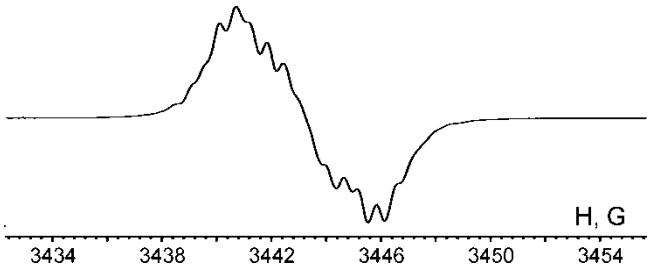

Figure S14. The isotropic X-band EPR spectrum of $[(Fc\text{-}IP)_2Sn^{IV}(4\text{-}Cl\text{-}3,6\text{-}SQ)]^+[Triflate]^-$ (**4**$^+$[Triflate]$^-$), g_i = 2.0036 (293 K, CH_2Cl_2).

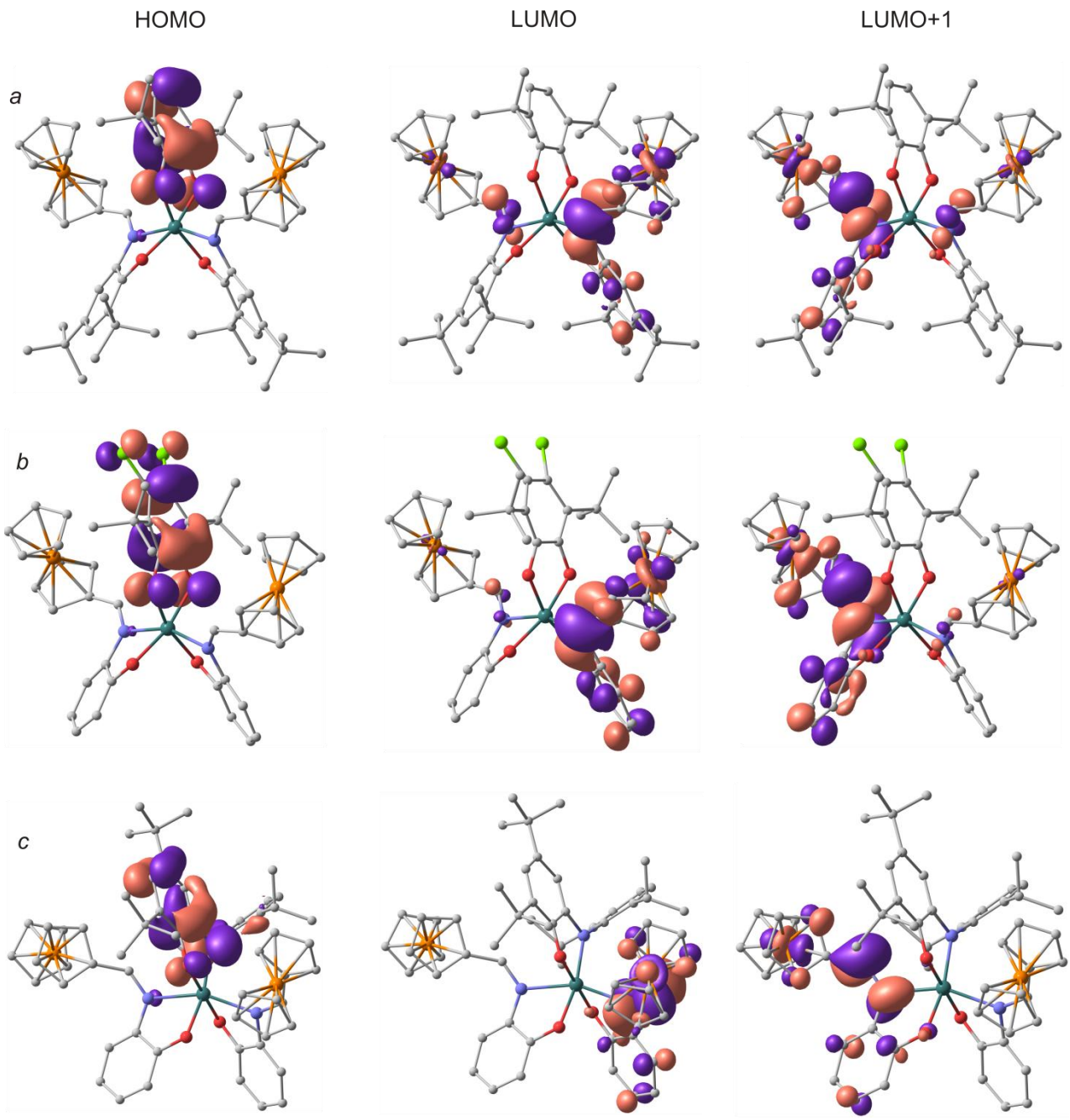

Figure S15. The shapes of frontier orbitals of complexes **1** (a), **6** (b) and **8** (c) calculated by the DFT B3LYP/6-31G(d, p)/SDD method. Hydrogen atoms are omitted for clarity, cutoff = 0.04 e/Å^3.